

# Nanospray Desorption Electrospray Ionization (nano-DESI) Mass Spectrometry Imaging of Drift Time-Separated Ions

Daisy Unsihuay,<sup>1</sup> Ruichuan Yin,<sup>1</sup> Daniela Mesa Sanchez,<sup>1</sup> Yingju Li,<sup>2</sup> Xiaofei Sun,<sup>2</sup> Sudhansu K. Dey,<sup>2</sup> Julia Laskin<sup>1\*</sup>

*1. Department of Chemistry, Purdue University, West Lafayette, IN 47907, USA*

*2. Division of Reproductive Sciences, Cincinnati Children's Hospital Medical Centre and Department of Pediatrics, University of Cincinnati College of Medicine, Cincinnati, OH, 45229, USA*

Corresponding author: Julia Laskin, Tel: 765-494-5464, Email: [jlaskin@purdue.edu](mailto:jlaskin@purdue.edu)

## ■ ABSTRACT

Simultaneous spatial localization and structural characterization of molecules in complex biological samples currently represents an analytical challenge for mass spectrometry imaging (MSI) techniques. In this study, we describe a novel experimental platform, which substantially expands the capabilities and enhances the depth of chemical information obtained in high spatial resolution MSI experiments performed using nanospray desorption electrospray ionization (nano-DESI). Specifically, we designed and constructed a portable nano-DESI MSI platform and coupled it with a drift tube ion mobility spectrometer-mass spectrometer (IM-MS). Separation of biomolecules observed in MSI experiments based on their drift times provides unique molecular descriptors necessary for their identification by comparison with databases. Furthermore, it enables isomer-specific imaging, which is particularly important for unraveling the complexity of biological systems. Imaging of day 4 pregnant mouse uterine sections using the newly developed nano-DESI-IM-MSI system demonstrates rapid isobaric and isomeric separation and reduced chemical noise in MSI experiments. A direct comparison of the performance of the new nano-DESI-MSI platform operated in the MS mode with the more established nano-DESI-Orbitrap platform indicates a comparable performance of these two systems. A spatial resolution of better than ~16  $\mu\text{m}$  and similar molecular coverage was obtained using both platforms. The structural information provided by the ion mobility separation expands the molecular specificity of high-resolution MSI necessary for the detailed understanding of biological systems.

## ■ INTRODUCTION

Mass spectrometry imaging (MSI) is ideally suited for the simultaneous mapping of the spatial distributions of hundreds of molecules directly from tissues in a label-free fashion.<sup>1–6</sup> MSI is widely used in biomedical research and drug discovery to obtain a better understanding of the molecular-level response of biological systems to different conditions. A majority of MSI applications are focused on the identification of biomarkers and monitoring disease progression,<sup>7–9</sup> understanding molecular alterations associated with organ development,<sup>10,11</sup> visualizing drug distributions in tissues to identify the mechanisms of their action,<sup>12,13</sup> and mapping the biological activity of enzymes by detecting their catalytic products.<sup>14</sup> Desorption electrospray ionization (DESI)<sup>15</sup> and matrix assisted laser desorption ionization (MALDI)<sup>16–18</sup> are the two most common soft ionization techniques used in MSI. Ambient ionization techniques like DESI have been employed in MSI experiments to eliminate sample pre-treatment prior to analysis and enable imaging of biological samples in their native state. Nanospray desorption electrospray ionization (nano-DESI) developed by our group<sup>19</sup> is an ambient liquid extraction-based ionization technique, which has been used for imaging of biological tissues with high sensitivity and high spatial resolution ( $\sim 10\ \mu\text{m}$ ).<sup>20</sup>

In the past two decades, substantial efforts have been dedicated to improving the spatial resolution, data processing and speed of analysis of MSI.<sup>5</sup> However, on-the-fly identification of molecules in MSI experiments is challenging. Furthermore, the presence of some isobaric and isomeric species, which cannot be separated by  $m/z$  alone complicates the interpretation of MSI data necessary for an improved molecular-level description of complex biological systems. Some of these challenges have been addressed using tandem mass spectrometry (MS/MS) imaging experiments, which enable simultaneous imaging and identification of molecules in biological samples.<sup>21,22</sup> However, these experiments are typically limited to a targeted list of  $m/z$  windows. Therefore, coupling MSI with structurally-sensitive techniques is a promising approach for the untargeted analysis with improved coverage and structural characterization of molecules in biological samples.

Ion mobility spectrometry (IMS) separates molecules based on their size, shape and charge<sup>23,24</sup> and operates on a millisecond time scale making it easy to integrate into MSI experiments.<sup>25,26</sup> Furthermore, drift tube ion mobility spectrometry (DTIMS) provides the structural information in the form of collision cross sections (CCS) of the separated ions.<sup>27–29</sup> An interlaboratory study has demonstrated that CCS values are reproducible across different experimental platforms,<sup>30</sup> which makes them excellent molecular descriptors and enables confident annotations of numerous biomolecules using open-source databases.<sup>31–33</sup>

Several ion mobility instruments have been successfully coupled with MSI techniques including MALDI,<sup>34,35</sup> DESI,<sup>36,37</sup> liquid extraction surface analysis (LESA),<sup>38</sup> laser desorption electrospray ionization (LAESI)<sup>39</sup> and infrared matrix-assisted laser desorption electrospray ionization (IR-MALDESI).<sup>40</sup> The advantages of such coupling include an improved molecular coverage and sensitivity, the ability to generate background-free images, and rapid isomeric separation.<sup>25,41</sup>

Herein, we describe the design and performance of a portable high-resolution nano-DESI imaging platform coupled to a linear ion mobility quadrupole time-of-flight mass spectrometer (IM-QTOF MS), which enables imaging of drift time-separated ions. Proof-of-concept MSI experiments using mouse uterine sections demonstrate the capabilities of this newly-developed platform for imaging of drift time-selected biomolecules with a spatial resolution ranging from 16 to 25  $\mu\text{m}$ . In combination with the previously reported quantitative capabilities of nano-DESI MSI, this platform opens up new research directions focused on isomer-selected quantitative imaging of complex biological samples. Furthermore, the newly developed versatile platform can be coupled to any type of a mass spectrometer making it broadly applicable to a variety of applications.

## ■ EXPERIMENTAL SECTION

### **Chemicals.**

Lysophosphatidylcholine (LPC 19:0) was purchased from Avanti Polar Lipids (Alabaster, AL). LC-MS grade methanol (MeOH) and water were purchased from Sigma-Aldrich (St. Louis, MO).

### **Tissue Samples.**

Uterine tissues on day 4 of pregnancy were retrieved from mice on a C57/BL6 mixed background as described in our previous studies.<sup>22,42</sup> The mice were housed in the Cincinnati Children's Hospital Medical Center Animal Care Facility according to National Institutes of Health and institutional guidelines for the use of laboratory animals and animal handling protocols of the approved by Cincinnati Children's Hospital Research Foundation Institutional Animal Care and Use Committee. Uterine tissues on day 4 of pregnancy were snap-frozen and sectioned using a cryostat. Sections of 12  $\mu\text{m}$  thickness were mounted onto glass slides and stored in a -80 C freezer prior to analysis.

### **Instrument description:**

Nano-DESI MSI experiments were performed on an Agilent 6560 IM-QTOF MS (Agilent Technologies, Santa Clara, CA) and Q-Exactive HF-X Orbitrap mass spectrometer (Thermo Fisher Scientific, Waltham,

MA). A custom-designed nano-DESI platform employed in the nano-DESI-Orbitrap experiments has been described in detail elsewhere.<sup>43–46</sup> Typical source conditions of the Q-Exactive HF-X are as follows: ESI voltage of +3.2 kV, capillary temperature of 250 °C, funnel RF level of 100.

A schematic of the nano-DESI source is shown in **Figure 1a**. **Figures 1b** and **1c** show the nano-DESI imaging system developed in this study which is assembled on a portable cart (1) that can be readily deployed in combination with any mass spectrometer. The cart houses all the components including a vibrationally insulated platform (2) (Newport, Irvine, CA), a lock-in amplifier (3) (Stanford Research Systems, Sunnyvale, CA) and a computer that controls the system (4). The XYZ stage (5) and sample holder are mounted on the vibrationally insulated platform, along with the micro-positioners (6) and Dino-Lite cameras (7). A stainless steel capillary extension (8) is attached to the mass spectrometer inlet as shown in **Figure 1c**. The nano-DESI probe is described in the next section. A pulse of 5V to 0V provided by the LabView program is used to synchronize the XYZ stage and Agilent’s acquisition software. Typical source parameters are as follows: ESI voltage of +4.5 kV, capillary temperature of 300 °C. Manual tuning was carried out to optimize the front funnel and rear funnel parameters in MS mode and IM mode. The detailed instrument settings can be found in **Tables S1-S3**. For nano-DESI IM-QTOF experiments, trapping time and release time were set to 15 ms and 150  $\mu$ s, respectively.

#### **Nano-DESI MSI:**

Imaging experiments were performed using a mixture of MeOH:H<sub>2</sub>O (9:1) (v/v), which was infused using a syringe pump (KD Scientific, Holliston, MA) at 0.5  $\mu$ L/min. The high-resolution nano-DESI probe is assembled in front of the mass spectrometer inlet as shown in **Figure 1** and described in our previous studies.<sup>43,46</sup> Briefly, the finely pulled primary (9) and spray (10) capillaries with OD of 15–25  $\mu$ m are aligned to form a liquid bridge. Analyte molecules are extracted into the liquid bridge directly from the tissue and transferred to a mass spectrometer inlet through the spray capillary. A third capillary (11), that serves as a shear-force probe,<sup>46</sup> is positioned in close proximity to the nano-DESI probe to maintain a constant distance between the sample and the nano-DESI probe. Mass spectra are acquired in positive mode in the range of  $m/z$  133–2000. Imaging data are acquired in lines by scanning the sample under the nano-DESI probe in one direction and stepping between the lines in another direction. For all the data reported in this study, we used a scan rate of 20  $\mu$ m/s and a step between the lines of 29  $\mu$ m resulting in a total analysis time of  $\sim$ 3 h per tissue section ( $\sim$ 4 mm<sup>2</sup>). To compare the performance of the nano-DESI-Orbitrap with nano-DESI-IM-QTOF operated in the MS mode, we used an acquisition rate of 7 Hz resulting in an average pixel size of  $2.9 \times 29 \mu\text{m}^2$ . Another series of experiments was performed to compare between

IM-QTOF and QTOF data using an acquisition rate of 1 Hz resulting in an average pixel size of  $20 \times 29 \mu\text{m}^2$ .

## Data processing

$[\text{M}+\text{Na}]^+$  and  $[\text{M}+\text{K}]^+$  ions are the most abundant species in positive mode nano-DESI MSI of biological tissues. The initial lipid and metabolite identifications are performed based on the accurate mass measurement using LIPID MAPS ([www.lipidmaps.org](http://www.lipidmaps.org)) and METLIN (<https://metlin.scripps.edu>). The final assignments are confirmed using MS/MS data collected over the tissue immediately after every imaging experiment using data-dependent acquisition (or auto MS/MS for QTOF). Moreover, the presence of multiple adducts of the same molecule is used to validate the assignments especially for the small metabolites, for which it is often difficult to find MS/MS spectra of alkali metal adducts in the literature.

Analysis of the nano-DESI-Orbitrap data is performed using the Peak-by-Peak software (Spectroswiss, Lausanne, Switzerland) that employs parallel (multi-core) calculations. A three-point quadratic interpolation to determine the apex of the peak is used to extract peaks from mass spectra. The abundance of selected  $m/z$  features in each pixel (mass spectrum) is normalized to the total ion current (TIC) and plotted as a function of the location on the tissue sample to generate ion images using a mass tolerance window of  $\pm 10$  ppm.

Analysis of the QTOF data is performed using the Ion Mobility-Mass Spectrometry Image Creator script developed by our group.<sup>47</sup> Though there is no ion mobility information in some of the current experiment unlike described in the original publication, the workflow still functions in the same fashion. In brief, the script interfaces with Skyline's<sup>48</sup> command line to input raw data files and export a chronogram summary of targeted masses. The script then reconstructs those chronograms into individual ion images. The resulting images use a self-normalized heat map color scale. Intensity values for each pixel are normalized to the TIC. For QTOF data, the mass list used to generate ion images are obtained using the peak list from averaged MS spectra of all lines. For data with mobility information, Agilent's MassHunter Mass Profiler software is used to extract a feature list, i.e. a list containing  $m/z$ , drift time, and charge information of recurring peaks among all experiment lines.

## ■ RESULTS AND DISCUSSION

Herein, we describe the implementation of high-resolution nano-DESI MSI on an Agilent 6560 IM-QTOF system. We evaluate the performance of nano-DESI-QTOF MSI by comparing the results obtained using the IM-QTOF system operated in the MS mode with the results obtained using the nano-DESI-Orbitrap system described in our previous studies.<sup>43,49</sup> Furthermore, we demonstrate the capabilities of nano-DESI

MSI in combination with IM separation, which enables both  $m/z$ - and ion mobility-selected imaging of molecules in tissues.

### Comparison of High-Resolution Nano-DESI MSI Performed on the QTOF and Orbitrap Systems.

**Figure 2a** shows representative mass spectra in the  $m/z$  range 700-900 acquired using nano-DESI-QTOF (top panel) and nano-DESI-Orbitrap (bottom panel). The spectra are averaged over a line scan corresponding to the central region of the uterine tissue. We observe that regardless of the platform used, phosphatidylcholine (PC) species are the dominant peaks in the  $m/z$  range 700-900 of uterine tissue in positive mode nano-DESI MSI. The major difference between the two spectra is the relative abundance of  $[M+Na]^+$  and  $[M+K]^+$  ions. Specifically,  $[M+Na]^+$  ions are more dominant in the Orbitrap spectrum, whereas  $[M+K]^+$  ions are more abundant in the QTOF spectrum. However, the same PC species are observed in both spectra. We attribute this difference to the variability between the tissue sections, which may have been collected from different regions of the uterine tissue. Alternatively, different rates of solvent evaporation from charged droplets in the heated inlets may affect the relative abundance of alkali metal adducts. For the purpose of comparison between the two nano-DESI platforms, we included only one adduct into the final count of the observed species. MS/MS data collected on the same tissue section after every imaging experiment, revealed the presence of isobaric compounds which could not be resolved neither by the Orbitrap ( $m/\Delta m = 46,369$  at  $m/z$  400.3415 and  $m/\Delta m = 34,474$  at  $m/z$  782.5653) nor by the QTOF ( $m/\Delta m = 20,636$  at  $m/z$  400.3415 and  $m/\Delta m = 23,465$  at  $m/z$  782.5653). Therefore, it is expected that ion images obtained for these peaks contain contributions from several overlapping species. Recently, it has been demonstrated that separation of the isobaric species can be improved using a Fourier transform ion cyclotron resonance mass spectrometer, an instrument, which has mass resolution far superior to the mass spectrometers employed in this work.<sup>50</sup> Alternatively, MS/MS imaging has been shown to separate isobaric species based on the unique fragments.<sup>22</sup>

Using nano-DESI MSI in positive mode, we have successfully detected 119 unique lipids across 15 lipid subclasses and 50 metabolites for a total of 169 identifications in mouse uterine tissue sections (**Figure 2b**). A complete list of the annotated species can be found in **Table S4**. PCs are by far the most abundant lipid subclass with the highest number of species (33 species), followed by PC plasmalogens (14 species) and diacylglycerols (DG, 14 species). Out of the 169 unique molecules identified, 158 species were detected with the Orbitrap and 148 with QTOF (**Figure 2c**). The main difference in the coverage displayed by these two platforms is in the number of phosphatidylethanolamine (PE) species, which is greater in the Orbitrap (13 species) than QTOF (3 species) data. PEs are zwitterionic compounds that can ionize in both positive and negative mode. However, they are not very abundant and are highly suppressed by PC species in

positive mode.<sup>51</sup> We attribute this difference in the number of PE species to the higher mass resolution of the Orbitrap, which helps resolve isobaric PE from PC species. For example, two neighboring ions at  $m/z$  818.5637 and 818.6019 were identified as sodiated PE(40:4) and PC(P-38:3), respectively. Separation of species with a mass difference of 0.0364 Da corresponding to the difference between  $\text{CH}_4$  and O, requires a mass resolution of 33,000 at  $m/z$  818.6019. This condition was met on the Orbitrap but not QTOF, which was operated in the extended dynamic range (2 GHz) mode. Therefore, a broad peak at  $m/z$  818.6015 was observed in the QTOF spectrum and was counted as PC(P-38:3), which excluded the isobaric PE(40:4) from the count.

**Figure 3** shows nano-DESI ion images collected using the Orbitrap (bottom row) and QTOF (top row) along with the optical images of the corresponding tissue sections. Different parts of the uterine section including myometrium (Myo), stroma (S), luminal epithelium (LE) and glandular epithelium (GE) are indicated in the optical image. Representative ion images of endogenous molecules highlight different patterns of region-specific molecular distributions observed in uterine tissue sections. For example, ion images corresponding to monoglyceride (MG) (18:1) and sphingomyelin (SM) (d34:1) display a substantial enhancement in the LE and GE cells. Meanwhile, a complementary distribution is observed for LPC(18:0) and PC(32:0) which are depleted in both LE and GE. A slight enhancement only in GE is observed for PC(36:5) and PC(36:4), whereas an enhancement only in LE is observed for PC(38:2). Most metabolites such as carnitine display a less delineated distribution and are distributed across stroma, LE, and GE. Finally, some molecules such as LPC(18:1) are evenly distributed across the entire tissue. Ion images of uterine tissue sections generated using the newly developed nano-DESI platform coupled to the QTOF, exhibit the same image quality and are in close agreement with the ion distributions obtained using the nano-DESI-Orbitrap system. Moreover, a spatial resolution of 15.8  $\mu\text{m}$  was calculated for QTOF ion images, which is comparable to the spatial resolution of 16.1  $\mu\text{m}$  displayed by the Orbitrap ion images (**Figure S1**). These results demonstrate the successful implementation of the high-resolution nano-DESI MSI on the IM-QTOF providing a path for obtaining high-quality ion images of drift time-separated species described in the next section. Furthermore, the portable platform presented herein enables the implementation of nano-DESI MSI on any commercial mass spectrometer. Indeed, we were able to use this platform in combination with an ion trap mass spectrometer in our laboratory.

#### **Nano-DESI MSI of Drift Time-Separated Ions**

In another experiment, we operated the IM-QTOF instrument in the IM-MS mode to enable IM separation of ions during nano-DESI MSI experiments. Nano-DESI IM-MSI experiments were performed using

mouse uterine sections with an acquisition rate of 1 Hz. For comparison, nano-DESI-MSI experiments were conducted using the same acquisition rate of 1 Hz.

**Figure 4a** shows the results of the positive mode nano-DESI molecular profiling obtained with and without the IM separation. A larger number of species was detected in the MS mode (146 species) than in the IM-MS mode (131 species). We attribute the difference in coverage between the two modalities to the overall loss in signal intensity in the IM-MS mode by about an order of magnitude in comparison with the MS mode. As a result, some low-abundance species including SM, MG, fatty acids (FA), and several metabolites were not detected in the IM-MS mode. Multiplexing strategies have proven to improve both the duty cycle and sensitivity of DTIMS systems.<sup>52–54</sup> We anticipate that a substantial improvement in the signal of low-abundant species and molecular coverage may be achieved by incorporating multiplexing into IM-MSI experiments.

**Figure 4b** displays drift time-separated ion images obtained for molecules in mouse uterine sections. The corresponding ion images obtained in the MS mode are shown for comparison. There is a good correspondence between the drift time-selected ion images and ion images obtained in the MS mode for the corresponding  $m/z$ . A slightly lower spatial resolution was obtained in both MS mode (23.4  $\mu\text{m}$ ) and IM-MS modes (25.3  $\mu\text{m}$ ) with an acquisition rate of 1 Hz in comparison to the results obtained at 7 Hz owing to the smaller number of mass spectra collected in a line scan (**Figure S1**). Indeed, we found that the sharpest chemical gradients in the 1 Hz data correspond to 1-2 pixels indicating that the spatial resolution in this experiment is determined by the acquisition rate rather than the size of the liquid bridge. However, as shown in **Figure S2**, the S/N ratio at 782.5655 is improved at slower acquisition rates from 915 at 7 Hz to 1699 at 1 Hz due to an increase in the number of mass spectra averaged per pixel.

**Figure 5a** shows the drift time vs.  $m/z$  plot of all the species identified in the mouse uterine tissue in nano-DESI-IM-MSI experiments. An expanded view of the  $m/z$  760-880 range shown in **Figure 5b** demonstrates how these molecules are grouped into different chemical families based on their drift times (DT). For each adduct type and lipid class indicated by different markers and colors in **Figure 5b**, we observe distinct homologous series of species differing by the number of double bonds. Each of these series is highlighted with a colored line and labeled using the AA:X notation, in which AA indicates the acyl chain length containing X double bonds. The number of double bonds in each species is indicated inside the corresponding marker in the plot. In order to simplify the information provided in **Figure 5b**, we removed protonated species as they showed overlapping trend lines with sodium adducts within the same class. A complete drift time vs.  $m/z$  plot, in which all the adducts are included is presented in **Figure S3**. Structural differences pertaining to the lipid class and type of adduct are easy to visualize based on the DT separation.



For example, it is relatively easy to distinguish different adducts of PC and PE species of varying length of fatty acyl tails. We observe that for the same length of acyl chains, PE species are characterized by shorter DTs indicating a better packing efficiency of these molecules in comparison to PCs.<sup>55</sup> Moreover, DT separation highlights structural changes within the same homologous series of species. For example, for the same lipid class, type of adduct, and acyl chain length, DTs decrease with increase in the degree of unsaturation. The addition of a double bond introduces a kink into the acyl chain which makes the molecule more compact and enables it to travel faster within the drift cell. These observations are consistent with the results reported in the literature<sup>56,57</sup> and highlight the power of IM separation for the identification of compounds observed in MSI experiments based on the predictable differences in the trend lines exhibited by every lipid class. Moreover, the ability to calculate CCS values directly from DT values is an advantage that will be exploited in future studies to improve the confidence of molecular annotations.

Detailed analysis of the IM-MSI data highlight several promising capabilities enabled by the nano-DESI-IM-QTOF platform. First, the ability to perform rapid isomeric differentiation on a time scale compatible with MSI experiments is critical to understanding the localization of isomeric species, which cannot be separated in MS mode. A representative 2D IM-MS plot for the  $m/z$  325.1-325.3 window is shown in **Figure S4**. We observe the presence of two isomeric components at  $m/z$  325.2108, which are readily separated by their DT. Ion images generated for these two components indicate different localization of the isomeric species in the tissue. The molecule at DT 25.87 ms is slightly enhanced in LE whereas the molecule at DT 26.83 ms is evenly distributed across the tissue. Although the identification of these species is beyond the scope of this paper, this result clearly illustrates that IM separation enables spatial localization of isomeric species. In combination with the structural information, which cannot be inferred from the accurate mass measurement alone, this capability is particularly advantageous for molecular-level understanding of biological processes.

Although some PC and PE species were not separated in the MS mode under the experimental conditions used in this study, they were readily separated in the IM mode. **Figure S5** shows a 2D IMS-MS map for the  $m/z$  818.4-818.7 window where the peaks at  $m/z$  818.5617 and  $m/z$  818.6011, which are not separated in the MS mode, are observed as two distinct features in the DT dimension. As a result, the number of PE species, for which ion images could be generated increased from 3 in the MS mode to 11 in the IM-MS mode (**Figure 4a**). This indicates that IM separation relaxes the constraints imposed on the mass resolving power of a mass spectrometer making MSI experiments more accessible to the scientific community. Previously, the isobaric differentiation in IM-MSI was used to distinguish between isobaric peptides fragments corresponding to tubulin and ubiquitin.<sup>58</sup> The reconstructed ion images of these proteins showed remarkably different distributions in rat brain tissue sections.

Another advantage provided by the IM separation is that it helps eliminate interferences from solvent peaks in nano-DESI MSI. **Figure S6** illustrates the separation of LPC(18:2) as a  $[M+Na]^+$  ion at  $m/z$  542.3208 from an isobaric solvent peak at  $m/z$  542.2983. It can be clearly observed that the spatial distribution of LPC(18:2) is completely masked by the background peak in the MS mode. Meanwhile, a distinct pattern showing that this molecule is depleted in both LE and GE is observed in the IM-MS mode. This capability has been previously used in MALDI-IMS-MSI experiments to obtain high-quality ion images of endogenous lipids in breast tumor tissue by reducing the interference from matrix ions.<sup>59</sup>

## ■ CONCLUSION

In this work, we expanded the analytical capabilities of nano-DESI MSI by successfully coupling it with ion mobility separation, which opens up new opportunities for the spatially-resolved analysis of complex biological samples. A new high-resolution nano-DESI source was developed, and its performance was evaluated in terms of coverage and quality of the obtained ion images. Using mouse uterine tissue as a model system, we demonstrate that similar molecular coverage, image quality, and spatial resolution are achieved using the new nano-DESI-QTOF platform and nano-DESI Orbitrap used in our previous studies. Moreover, the newly developed nano-DESI platform is portable and can be interfaced with any commercial mass spectrometer. Nano-DESI-IM-MSI experiments provide mass- and drift time-selected ion images of uterine sections with high spatial resolution. Coupling of ion mobility separation with nano-DESI MSI improves the separation of both isobaric and isomeric species thereby increasing the molecular specificity of imaging experiments. Moreover, drift time separation eliminates the unwanted contribution of background peaks to the observed ion images of endogenous molecules extracted from the sample. Future studies will focus on improving sensitivity of the IM-MSI experiments to enable the detection of low-abundance species. This can be achieved using multiplexing strategies, which improve the sensitivity of IM experiments at no expense of the throughput. Our first proof-of-concept experiments indicate that the new nano-DESI-IM-MSI platform improves the depth of structural information of interest to biological and clinical research.

## ■ ACKNOWLEDGMENTS

This research is supported by the grant from the National Science Foundation (NSF-1808136, JL) and National Institute of Health (HD068524, SKD). DMS acknowledges support from the National Science Foundation Graduate Research Fellowship under Grant No. (DGE-1333468). Any opinions, findings, and conclusions or recommendations expressed in this material are those of the authors and do not necessarily reflect the views of the NSF or NIH. We would like to thank to Pei Su, Dr. Ruwan T. Kurulugama, and Dr.

John Fjeldsted for their technical assistance with the QTOF instrument and data analysis workflow used in this study.

## ■ ASSOCIATED CONTENT

Supporting Information. The Supporting Information is available free of charge on the ACS Publications website.

## ■ AUTHOR INFORMATION

Corresponding Author

\*Phone: 765-494-5464. E-mail: [jlaskin@purdue.edu](mailto:jlaskin@purdue.edu)

Notes

The authors declare no competing financial interest.

## ■ REFERENCES

- (1) Stoeckli, M.; Chaurand, P.; Hallahan, D. E.; Caprioli, R. M. *Nat. Med.* **2001**, 7, 493–496.
- (2) Wu, C.; Dill, A. L.; Eberlin, L. S.; Cooks, R. G.; Ifa, D. R. *Mass Spectrom. Rev.* **2013**, 32 (3), 218–243.
- (3) Nilsson, A.; Goodwin, R. J. A.; Shariatgorji, M.; Vallianatou, T.; Webborn, P. J. H.; Andrén, P. E. *Anal. Chem.* **2015**, 87, 1437–1455.
- (4) Lanni, E. J.; Rubakhin, S. S.; Sweedler, J. V. *J. Proteomics* **2012**, 75 (16), 5036–5051.
- (5) Buchberger, A. R.; DeLaney, K.; Johnson, J.; Li, L. *Anal. Chem.* **2018**, 91 (8), 240–265.
- (6) McDonnell, L. A.; Heeren, R. M. A. *Mass Spectrom. Rev.* **2007**, 26 (4), 606–643.
- (7) Tsubata, Y.; Hayashi, M.; Tanino, R.; Aikawa, H.; Ohuchi, M.; Tamura, K.; Fujiwara, Y.; Isobe, T.; Hamada, A. *Sci. Rep.* **2017**, 7, 12622.
- (8) Jarmusch, A. K.; Pirro, V.; Baird, Z.; Hattab, E. M.; Cohen-Gadol, A. A.; Cooks, R. G. *Proc. Natl. Acad. Sci. U. S. A.* **2016**, 113 (6), 1486–1491.
- (9) Lanekoff, I.; Cha, J.; Kyle, J. E.; Dey, S. K.; Laskin, J.; Burnum-Johnson, K. E. *Sci. Rep.* **2016**, 6, 33023.
- (10) Garikapati, V.; Karnati, S.; Bhandari, D. R.; Baumgart-Vogt, E.; Spengler, B. *Sci. Rep.* **2019**, 9, 3192.
- (11) Dautel, S. E.; Kyle, J. E.; Clair, G.; Sontag, R. L.; Weitz, K. K.; Shukla, A. K.; Nguyen, S. N.; Kim, Y. M.; Zink, E. M.; Luders, T.; Frevert, C. W.; Gharib, S. A.; Laskin, J.; Carson, J. P.; Metz, T. O.; Corley, R. A.; Ansong, C. *Sci. Rep.* **2017**, 7, 40555.
- (12) Bruinen, A. L.; Van Oevelen, C.; Eijkel, G. B.; Van Heerden, M.; Cuyckens, F.; Heeren, R. M. A. *J. Am. Soc. Mass Spectrom.* **2016**, 27 (1), 117–123.

- 345 (13) Rao, T.; Shao, Y.; Hamada, N.; Li, Y.; Ye, H.; Kang, D.; Shen, B.; Li, X.; Yin, X.; Zhu, Z.; Li, H.;  
346 Xie, L.; Wang, G.; Liang, Y. *Anal. Chim. Acta* **2017**, 952, 71–80.
- 347 (14) Hamilton, B. R.; Marshall, D. L.; Casewell, N. R.; Harrison, R. A.; Blanksby, S. J.; Undheim, E.  
348 A. B. *Angew. Chemie - Int. Ed.* **2020**, 59, 3855–3858.
- 349 (15) Eberlin, L. S.; Ferreira, C. R.; Dill, A. L.; Ifa, D. R.; Cooks, R. G. *Biochim. Biophys. Acta - Mol.*  
350 *Cell Biol. Lipids* **2011**, 1811 (11), 946–960.
- 351 (16) Spengler, B. *Anal. Chem.* **2015**, 87 (1), 64–82.
- 352 (17) Gode, D.; Volmer, D. A. *Analyst* **2013**, 138 (5), 1289–1315.
- 353 (18) Cornett, D. S.; Reyzer, M. L.; Chaurand, P.; Caprioli, R. M. *Nat. Methods* **2007**, 4, 828–833.
- 354 (19) Roach, P. J.; Laskin, J.; Laskin, A. *Analyst* **2010**, 135, 2233–2236.
- 355 (20) Laskin, J.; Heath, B. S.; Roach, P. J.; Cazares, L.; Semmes, O. J. *Anal. Chem.* **2012**, 84 (1), 141–  
356 148.
- 357 (21) Burnum, K. E.; Cornett, D. S.; Puolitaival, S. M.; Milne, S. B.; Myers, D. S.; Tranguch, S.;  
358 Brown, H. A.; Dey, S. K.; Caprioli, R. M. *J. Lipid Res.* **2009**, 50 (11), 2290–2298.
- 359 (22) Lanekoff, I.; Burnum-Johnson, K.; Thomas, M.; Short, J.; Carson, J. P.; Cha, J.; Dey, S. K.; Yang,  
360 P.; Prieto Conaway, M. C.; Laskin, J. *Anal. Chem.* **2013**, 85 (20), 9596–9603.
- 361 (23) Paglia, G.; Astarita, G. *Nat. Protoc.* **2017**, 12, 797–813.
- 362 (24) Dodds, J. N.; Baker, E. S. *J. Am. Soc. Mass Spectrom.* **2019**, 30 (11), 2185–2195.
- 363 (25) Kiss, A.; Heeren, R. M. A. *Anal. Bioanal. Chem.* **2011**, 399, 2623–2634.
- 364 (26) Sans, M.; Feider, C. L.; Eberlin, L. S. *Curr. Opin. Chem. Biol.* **2018**, 42, 138–146.
- 365 (27) May, J. C.; Goodwin, C. R.; Lareau, N. M.; Leaptrot, K. L.; Morris, C. B.; Kurulugama, R. T.;  
366 Mordehai, A.; Klein, C.; Barry, W.; Darland, E.; Overney, G.; Imatani, K.; Stafford, G. C.;  
367 Fjeldsted, J. C.; McLean, J. A. *Anal. Chem.* **2014**, 86 (4), 2107–2116.
- 368 (28) Bowers, M. T. *Int. J. Mass Spectrom.* **2014**, 370, 75–95.
- 369 (29) Bohrer, B. C.; Merenbloom, S. I.; Koeniger, S. L.; Hilderbrand, A. E.; Clemmer, D. E. *Annu. Rev.*  
370 *Anal. Chem.* **2008**, 1, 293–327.
- 371 (30) Stow, S. M.; Causon, T. J.; Zheng, X.; Kurulugama, R. T.; Mairinger, T.; May, J. C.; Rennie, E.  
372 E.; Baker, E. S.; Smith, R. D.; McLean, J. A.; Hann, S.; Fjeldsted, J. C. *Anal. Chem.* **2017**, 89 (17),  
373 9048–9055.
- 374 (31) Picache, J. A.; Rose, B. S.; Balinski, A.; Leaptrot, K. L.; Sherrod, S. D.; May, J. C.; McLean, J. A.  
375 *Chem. Sci.* **2019**, 10, 983–993.
- 376 (32) Zheng, X.; Aly, N. A.; Zhou, Y.; Dupuis, K. T.; Bilbao, A.; Paurus, V. L.; Orton, D. J.; Wilson,  
377 R.; Payne, S. H.; Smith, R. D.; Baker, E. S. *Chem. Sci.* **2017**, 8, 7724–7736.
- 378 (33) Plante, P. L.; Francovic-Fontaine, É.; May, J. C.; McLean, J. A.; Baker, E. S.; Laviolette, F.;  
379 Marchand, M.; Corbeil, J. *Anal. Chem.* **2019**, 91 (8), 5191–5199.
- 380 (34) Jackson, S. N.; Ugarov, M.; Egan, T.; Post, J. D.; Langlais, D.; Schultz, J. A.; Woods, A. S. *J.*  
381 *Mass Spectrom.* **2007**, 42 (8), 1093–1098.

- 382 (35) Spraggins, J. M.; Djambazova, K. V.; Rivera, E. S.; Migas, L. G.; Neumann, E. K.; Fuetterer, A.;  
383 Suetering, J.; Goedecke, N.; Ly, A.; Van De Plas, R.; Caprioli, R. M. *Anal. Chem.* **2019**, *91* (22),  
384 14552–14560.
- 385 (36) Feider, C. L.; Elizondo, N.; Eberlin, L. S. *Anal. Chem.* **2016**, *88* (23), 11533–11541.
- 386 (37) Bennett, R. V.; Gamage, C. M.; Galhena, A. S.; Fernández, F. M. *Anal. Chem.* **2014**, *86* (8), 3756–  
387 3763.
- 388 (38) Griffiths, R. L.; Hughes, J. W.; Abbatiello, S. E.; Belford, M. W.; Styles, I. B.; Cooper, H. J. *Anal.*  
389 *Chem.* **2020**, *92* (4), 2885–2890.
- 390 (39) Shrestha, B.; Vertes, A. *Anal. Chem.* **2014**, *86* (9), 4308–4315.
- 391 (40) Ekelöf, M.; Dodds, J.; Khodjaniyazova, S.; Garrard, K. P.; Baker, E. S.; Muddiman, D. C. *J. Am.*  
392 *Soc. Mass Spectrom.* **2020**, *31* (3), 642–650.
- 393 (41) Sans, M.; Feider, C. L.; Eberlin, L. S. *Curr. Opin. Chem. Biol.* **2018**, *42*, 138–146.
- 394 (42) Lanekoff, I.; Burnum-Johnson, K.; Thomas, M.; Cha, J.; Dey, S. K.; Yang, P.; Prieto Conaway, M.  
395 C.; Laskin, J. *Anal. Bioanal. Chem.* **2015**, *407* (8), 2063–2071.
- 396 (43) Yin, R.; Burnum-Johnson, K. E.; Sun, X.; Dey, S. K.; Laskin, J. *Nat. Protoc.* **2019**, *14* (12), 3445–  
397 3470.
- 398 (44) Lanekoff, I.; Heath, B. S.; Liyu, A.; Thomas, M.; Carson, J. P.; Laskin, J. *Anal. Chem.* **2012**, *84*  
399 (19), 8351–8356.
- 400 (45) Nguyen, S. N.; Sontag, R. L.; Carson, J. P.; Corley, R. A.; Ansong, C.; Laskin, J. *J. Am. Soc. Mass*  
401 *Spectrom.* **2018**, *29* (2), 316–322.
- 402 (46) Nguyen, S. N.; Liyu, A. V.; Chu, R. K.; Anderton, C. R.; Laskin, J. *Anal. Chem.* **2017**, *89* (2),  
403 1131–1137.
- 404 (47) Mesa Sanchez, D.; Creger, S.; Singla, V.; Kurulugama, R. T.; Fjeldsted, J.; Laskin, J. *J. Am. Soc.*  
405 *Mass Spectrometry submitted*.
- 406 (48) MacLean, B.; Tomazela, D. M.; Shulman, N.; Chambers, M.; Finney, G. L.; Frewen, B.; Kern, R.;  
407 Tabb, D. L.; Liebner, D. C.; MacCoss, M. J. *Bioinformatics* **2010**, *26* (7), 966–968.
- 408 (49) Yin, R.; Kyle, J.; Burnum-Johnson, K.; Bloodsworth, K. J.; Sussel, L.; Ansong, C.; Laskin, J.  
409 *Anal. Chem.* **2018**, *90* (11), 6548–6555.
- 410 (50) Bowman, A. P.; Blakney, G. T.; Hendrickson, C. L.; Ellis, S. R.; Heeren, R. M. A.; Smith, D. F.  
411 **2020**, *92* (4), 3133–3142.
- 412 (51) Boskamp, M. S.; Soltwisch, J. *Anal. Chem.* **2020**, *92* (7), 5222–5230.
- 413 (52) Clowers, B. H.; Belov, M. E.; Prior, D. C.; Danielson, W. F.; Ibrahim, Y.; Smith, R. D. *Anal.*  
414 *Chem.* **2008**, *80* (7), 2464–2473.
- 415 (53) Groessl, M.; Graf, S.; Taylor, A.; Knochenmuss, R. **2015**, 1–4.
- 416 (54) Zheng, X.; Wojcik, R.; Zhang, X.; Ibrahim, Y. M.; Burnum-Johnson, K. E.; Orton, D. J.; Monroe,  
417 M. E.; Moore, R. J.; Smith, R. D.; Baker, E. S. *Annu. Rev. Anal. Chem.* **2017**, *10* (1), 71–92.
- 418 (55) Hines, K. M.; May, J. C.; McLean, J. A.; Xu, L. *Anal. Chem.* **2016**, *88*, 7329–7336.

419 (56) Jackson, S. N.; Ugarov, M.; Post, J. D.; Egan, T.; Langlais, D.; Schultz, J. A.; Woods, A. S. *J. Am.*  
420 *Soc. Mass Spectrom.* **2008**, *19* (11), 1655–1662.

421 (57) Leaptrot, K. L.; May, J. C.; Dodds, J. N.; McLean, J. A. *Nat. Commun.* **2019**, *10* (1), 985.

422 (58) Stauber, J.; MacAleese, L.; Franck, J.; Claude, E.; Snel, M.; Kaletas, B. K.; Wiel, I. M. V. D.;  
423 Wisztorski, M.; Fournier, I.; Heeren, R. M. A. *J. Am. Soc. Mass Spectrom.* **2010**, *21* (3), 338–347.

424 (59) Chughtai, K.; Jiang, L.; Greenwood, T. R.; Glunde, K.; Heeren, R. M. A. *J. Lipid Res.* **2013**, *54*  
425 (2), 333–344.

426

427

428

429

430

431

432

433

434

435

436

437

438

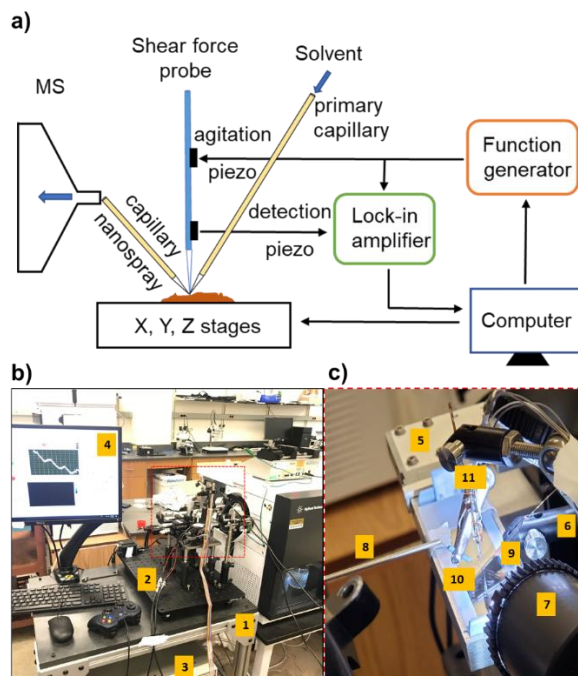


**Figure 1.** **a)** A schematic drawing of the nano-DESI MSI source from ref<sup>43</sup>. **b)** A photograph of the imaging platform, showing the custom-designed cart (1); vibrationally insulated platform (2); lock-in amplifier (3), and computer that controls the xyz stage (4). **c)** A zoomed-in photograph corresponding to the red dashed box in panel b. The XYZ stage (5), micro positioners (6), Dino-Lite microscope (7), capillary extension (8), primary capillary (9), spray capillary (10) and shear force probe (11) are also highlighted.

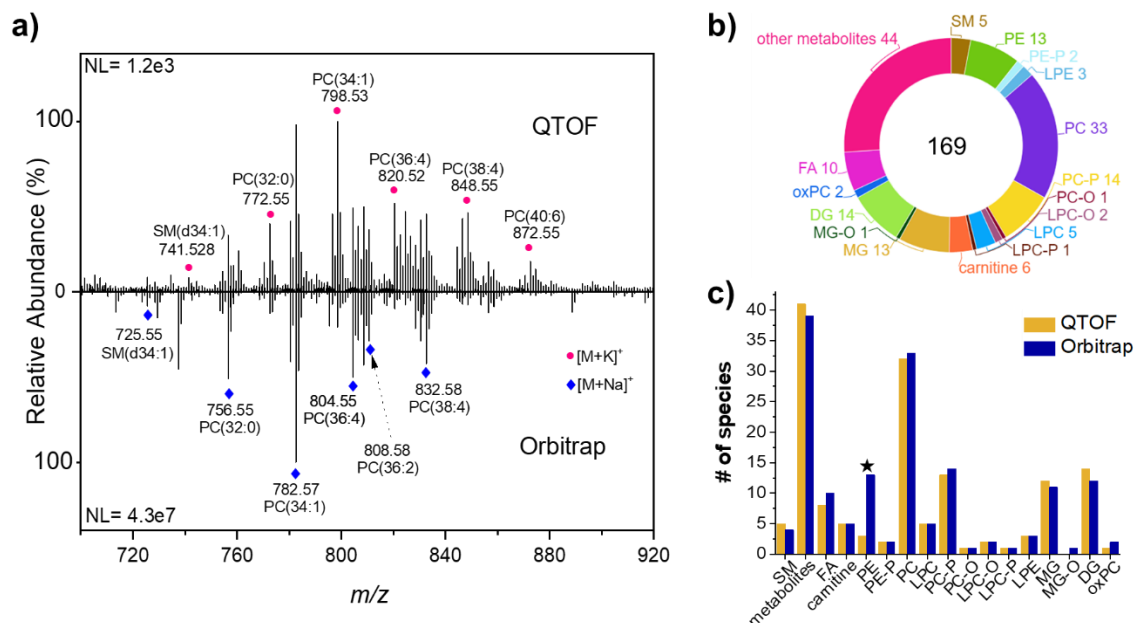


**Figure 2. a)** Mass spectra averaged over a linescan across the central region of a mouse uterine section (red dashed line) shown in the optical image. The spectrum acquired using QTOF is shown as positive signal and the spectrum acquired using an Orbitrap is shown as negative signal. Pink circles and blue diamonds denote  $[M+K]^+$  and  $[M+Na]^+$  ions, respectively. **b)** Pie chart showing the total number of species detected from the molecular profiling in positive mode with both platforms. **c)** Direct comparison of the number of species detected by molecular class with the QTOF and Orbitrap imaging platforms.



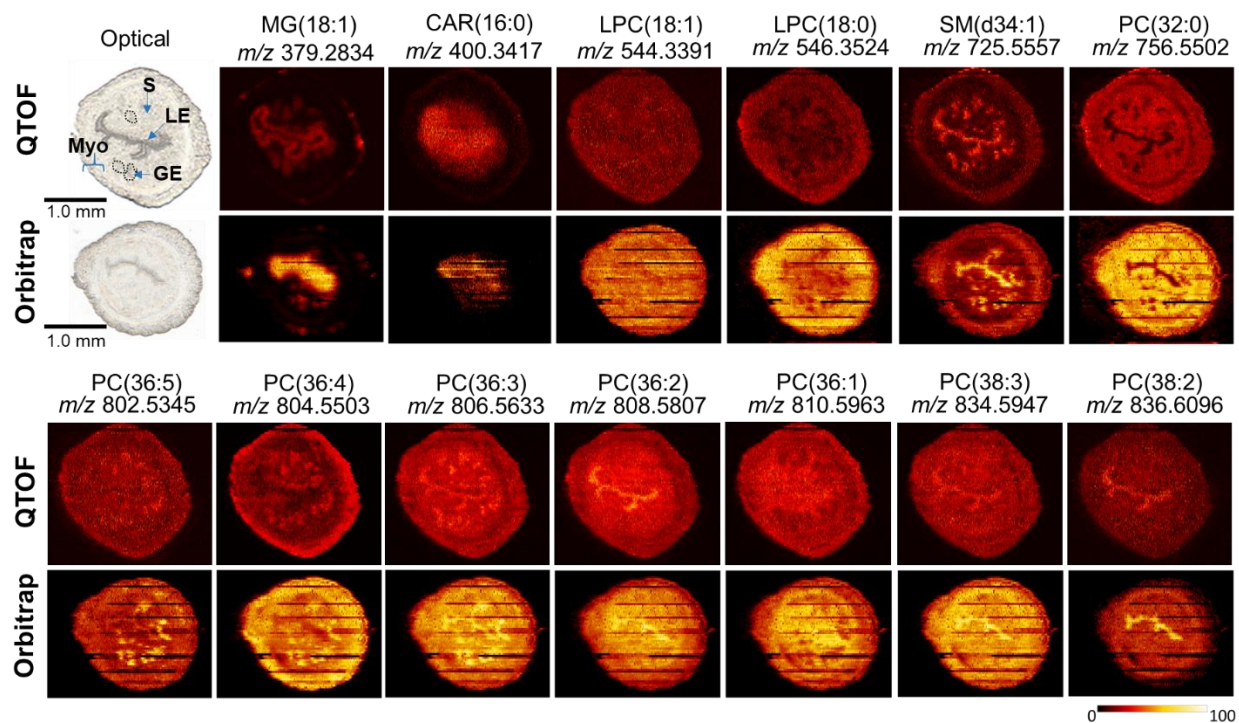


**Figure 3.** Representative nano-DESI ion images from mouse uterine sections collected using the new nano-DESI-QTOF platform (top row) and the traditional nano-DESI-orbitrap platform (bottom row). These data sets were collected using 7 Hz acquisition rate. Optical images of the uterine tissue sections highlighting their main components like myometrium (myo), stroma (S), luminal epithelium (LE) and glandular epithelium (GE) are included on the left side. The intensity scale changes from black (low) to yellow (high).

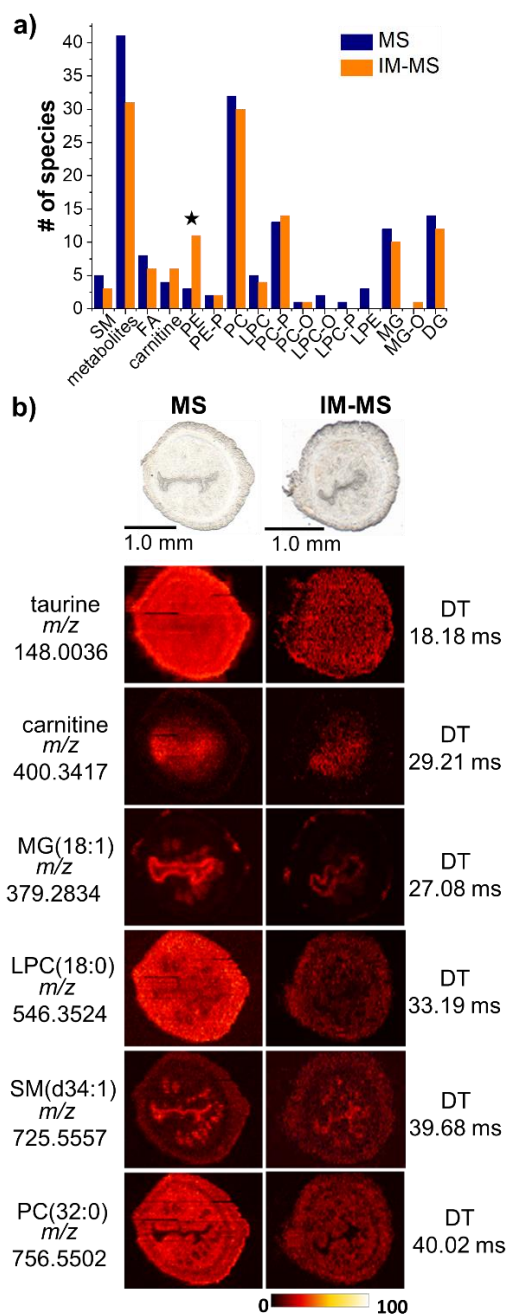


**Figure 4. a)** Direct comparison of the number of species in each molecular class detected in mouse uterine sections using the MS and IM-MS modes of the IM-QTOF instrument. **b)** Representative ion images of endogenous molecules of mobility separated ions using the nano-DESI-IM-QTOF platform (right column). Ion images collected without mobility separation are included in the left column for comparison. Optical images of the uterine tissue sections used for imaging experiments are shown in the first row. The intensity scale changes from black (low) to yellow (high).

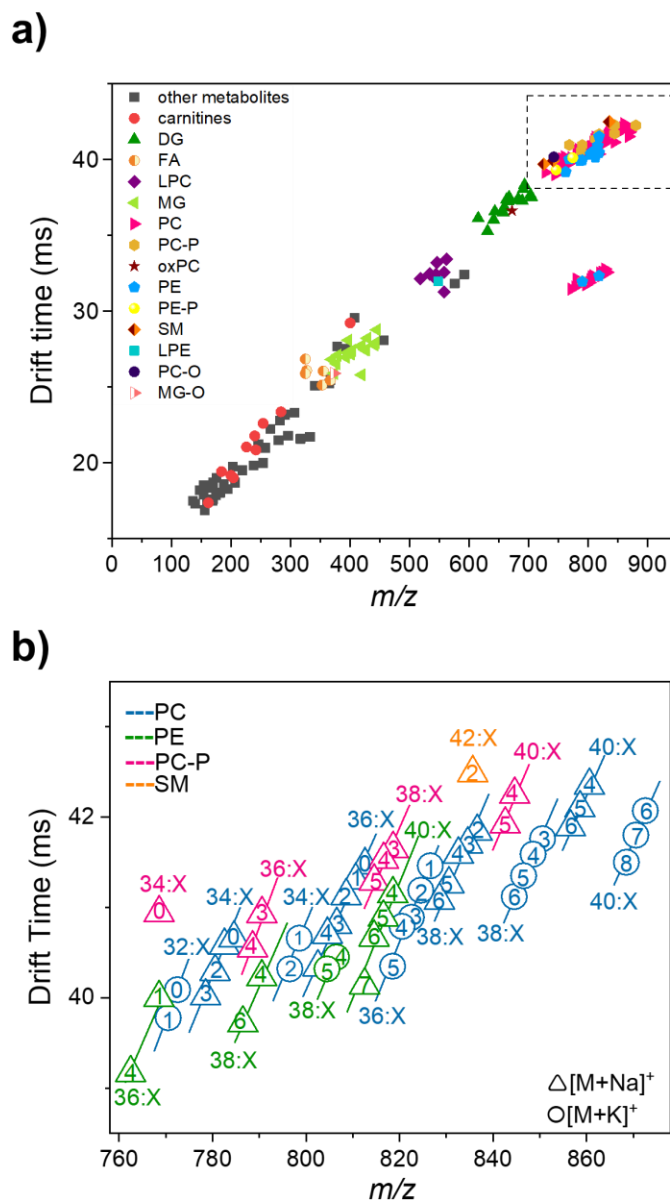
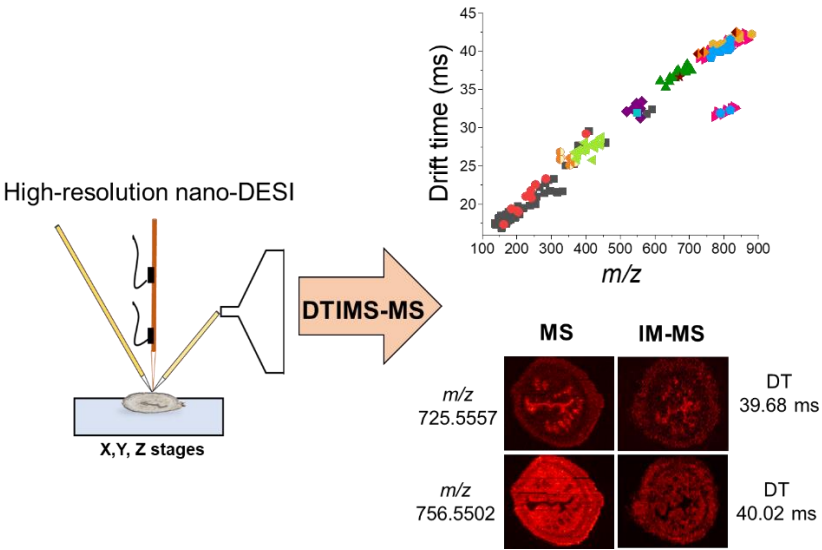


**Figure 5. a)** Drift time vs.  $m/z$  plot of the species identified in the nano-DESI-IM-MSI data. **b)** Lipid classes separated by drift time in the  $m/z$  760-880 region highlighted with the dashed box in panel. Triangles and circles denote  $[M+Na]^+$  and  $[M+K]^+$ , respectively and the symbol colors indicate the lipid class of the molecule as indicated in the legend. The nomenclature used to indicate the individual species is AA:X, where AA denotes the acyl chain length and X denotes the number of double bonds. The colored lines highlight the series of homologous species differing by the number of double bonds; the number of double bonds for each species is indicated inside the corresponding marker.

488

489

490   **For Table of Contents Only**



491